The Role of Outflow-Layer Instabilities in Tropical Cyclone Motion

MARIA FLATAU

Department of Atmospheric Science, Colorado State University, Fort Collins, Colorado

DUANE E. STEVENS

Department of Meteorology, University of Hawaii, Honolulu, Hawaii

(Manuscript received 27 February 1992, in final form 1 September 1992)

ABSTRACT

The paper examines the role of the development of outflow-layer instabilities on the motion of tropical cyclones. The influence of barotropic instability is examined by comparing the time changes in the storm tracks with the frequencies of free, unstable barotropic modes. For intense vortices barotropic instability is shown to contribute to the slow (periods of a few days) trochoidal motion of a cyclone. The development of instability depends on the horizontal distribution and frequency of environmental forcing. The strongest response occurs when the frequency of the forcing matches the frequency of an unstable mode.

1. Introduction

The goal of this study is to examine the dynamic processes in the tropical cyclone outflow layer and their influence on cyclone motion. The paper is an extension of our earlier work (Flatau and Stevens 1989) on the development of outflow-layer instabilities. In Flatau and Stevens (1989), we have shown that in a shallow-water model describing the outflow layer of a tropical cyclone, inertially and barotropically unstable perturbations develop. Barotropically unstable modes obtained in a shallow-water model revealed some features observed in tropical cyclones. For example, the most unstable modes occurred for small azimuthal wavenumbers, with the largest growth rates for $s = 1$. The structure of the most unstable modes resembled the outflow channels from Black and Anthes (1971).

The fact that we found barotropic instability to have its largest growth rate for $s = 1$ azimuthal wavenumber suggests that development of barotropic instability can influence the motion of a tropical cyclone. The indication of such an influence was present in one-layer models of tropical cyclone motion where tropical cyclones were represented by barotropic cyclonic vortices (Willoughby 1988; Peng and Williams 1990). For example, Willoughby (1988) in his shallow-water linear model observed a sudden change in calculated vortex movement if the frequency of the external forcing matched the maximum anticyclonic angular velocity in the vortex. Willoughby explained this effect by the resonance between the forcing and the free barotropically unstable mode. In their barotropic model, Peng and Williams (1990) noticed the presence of perturbations with a structure similar to that of barotropically unstable modes.

It is not clear how the unstable modes observed in one-layer models relate to the motion of a baroclinic vortex. One of the drawbacks of one-layer models is that the mean tangential flow is assumed a priori. The vortices used in these models to represent the tropical cyclones usually have the anticyclonic circulation at large radii that results from the demand that the total relative angular momentum of the vortex L_R be equal to zero [as shown by DeMaria (1987), assuming that $L_R = 0$ for the initial vortex reduces the errors in numerical prediction of hurricane movement based on a barotropic model]. As a consequence, there is a region in the vortex with reversed vorticity gradient, so the flow satisfies the necessary condition for barotropic instability. In reality, we do not know if the low-level flow is barotropically unstable. The conditions for barotropic instability are more likely to be met in the upper troposphere (Schubert and Alworth 1987), and as shown in Flatau and Stevens (1989), barotropically unstable modes develop in this layer. The question arises as to what extent the processes in the outflow layer can influence the motion of the entire vortex.

In this paper, we study the development of barotropically unstable modes in a three-dimensional, nonlinear model of a moving baroclinic vortex. The tangential flow in this model develops as a result of a prescribed diabatic heating. In contrast to our shallow-water model, the three-dimensional model is not iso-

Corresponding author address: Dr. Maria Flatau, Scripps Institution of Oceanography, University of California, San Diego, La Jolla, CA 92093-0239.

lated from the environment, and simple forms of external forcing are taken into account. In the framework of this model, we examine how the motion of the entire vortex depends on dynamical processes in the upper, unstable layer.

2. Numerical model

Our baroclinic vortex model uses the nonlinear, primitive equations. The equations are formulated on a β plane, but in this paper we assume $\beta = 0$. Cylindrical coordinates in the horizontal and the $\sigma = p/p_s$ coordinate in the vertical are used. The model consists of five equally spaced layers. There is no boundary layer, but we include energy sinks in the form of Newtonian friction in the lowest layer and uniform Rayleigh cooling. Horizontal velocities and potential temperature are defined in the middle of each layer, whereas the vertical velocity, $\dot{\sigma}$, is staggered. Following Hack and Schubert (1980), we use the Arakawa vertical differencing scheme.

The model is half-spectral with a Fourier representation in the azimuthal direction. All the model variables are expressed as

$$X(r, \lambda, \sigma) = \sum_{s=-S}^{S} x_s(r, \sigma) \exp(is\lambda). \quad (1)$$

This representation allows us to limit the number of tangential modes necessary to describe three-dimensional features of a moving vortex. Since many characteristics of an environmental flow that are important to the vortex motion (e.g., horizontally uniform flow or planetary vorticity gradient) have $s = 1$ azimuthal structure, even linear models, including only one tangential asymmetric component, can give some insight into the processes governing the vortex motion (Willoughby 1988; Peng and Williams 1990). Our previous analysis of dynamic instabilities in the hurricane outflow layer (Flatau and Stevens 1989) shows that asymmetries that develop in an outflow layer of an isolated hurricane have low azimuthal wavenumbers. The amplitude of these asymmetries decreases with increasing tangential wavenumber and practically approaches zero for $s > 2$. Therefore, for most of our experiments, four (0, 1, 2, 3) tangential wavenumbers are considered. If the problem demands higher azimuthal resolution, more tangential components can be used.

Because of the low number of spectral components, all calculations are carried out in spectral space, and interaction coefficients for nonlinear terms are explicitly determined. Generally for spectral models, calculating interaction coefficients is very inefficient, and transform methods utilizing FFTs are preferred. In our model, however, where the spectral representation is used only in one direction and the number of spectral coefficients is small, using the FFT does not provide any real advantages. The nonlinear terms in the governing equations include multiplications of two variables as well as raising p_s (surface pressure) to a real power w ($w = R/c_p$ in potential temperature definition and $w = -1$ when variables are divided by surface pressure). Since the symmetric part of the surface pressure p_{ss} is much larger than the asymmetric part p_{sa}, we use the Taylor expansion:

$$p_s^w = p_{ss}^w \left(1 + \frac{p_{sa}}{p_{ss}} w + \frac{1}{2!} \frac{p_{sa}^2}{p_{ss}^2} w(w-1) \cdots \right). \quad (2)$$

Because $p_{ss} \gg p_{sa}$ and because we use only three spectral components, the procedure converges quickly, and only a few terms in the Taylor expansion are needed.

In the modeling of vortex–environment interaction a large domain needs to be used. At the same time the area close to the cyclone center has to be resolved with a relatively fine grid. In primitive equation models nested grids are usually used, with the finest grid following the moving vortex (Jones 1977; Kitade 1980). In balanced models (Schubert and Hack 1983; Emanuel 1989) using potential radius as a radial coordinate provides natural coordinate stretching in the areas of large vorticity. Since in our model the use of spectral representation provides increased tangential resolution near the vortex center, only the radial coordinate needs to be modified. The model equations are transformed to the new coordinate $\hat{r}$, defined as

$$\hat{r}(r) = (r + r_a)^{1/\gamma}. \quad (3)$$

For γ larger than one, and uniformly spaced $\hat{r}$, the radial resolution increases with decreasing radius. The shift by r_a was used to avoid infinite derivatives at $r = 0$. In calculations described in this paper, $\gamma = 1.8$, $R_{\max} = 3200$ km (radius of the domain), and $N = 50$ (number of grid points). This choice of parameters gives 23-km resolution near the vortex center and about 100-km resolution at the outer boundary. The computational domain is divided into two parts. The inner part consists of a circle with radius $R_i = 1500$ km. A ring between R_i and $R_{\max}$ forms an outer part of the domain, which acts as a "sponge layer" for the inner part. In this layer the prognostic variables are relaxed toward the prescribed environmental values.

The model is formulated in a stationary coordinate system. Such formulation causes two problems. The first, similar to that encountered in nested grids models, is that the center of the vortex "escapes" from the area where the coordinate stretching and Fourier expansion provide the finest resolution. The other problem results from using a spectral representation of the variables. When the vortex center is too far from the coordinate center, the asymmetries are mainly the result of this displacement and not of the vortex dynamics. This is an especially undesirable feature in the case of the pressure field. Since we use the Taylor expansion to calculate some of the nonlinear terms involving the surface pressure, it is quite important that the surface

pressure field be as symmetric as possible. To deal with these problems, we use a procedure similar to that in Jones (1977) and relocate the coordinate center to match the vortex center if the distance between them exceeds the prescribed limit r_d. The definition of the vortex center is based on the surface pressure field. In observations, the surface pressure contours close to the cyclone center nearly approximate a circle. Therefore, to calculate the vortex center we choose the pressure contour, fit the circle to this contour using the least-squares method, and define the vortex center as a center of such a circle. That way, the asymmetric component of the pressure field is minimized. Choosing different pressure contours gives similar results, but care must be taken to choose a closed contour.

The model equations do not include moist processes explicitly, and the diabatic heat source is specified. We assume that the heat source is symmetric with respect to the vortex center. Following Hack and Schubert (1986), the heating function approximates the apparent heat source from Yanai et al. (1973) and has the form

$$Q = a\hat{Q} \sin(\pi\sigma) \exp(-\alpha\sigma) \exp(-r^2/r_0^2), \quad (4)$$

where $\hat{Q} = 7.87°\text{C day}^{-1}$, $\alpha = 0.554$, $r_0 = 150$ km. We assume that the magnitude of the heat source does not change with time and that the distribution is constant relative to the vortex center (not the coordinate center). The energy sinks in the model include Newtonian friction in the lowest layer and uniform Rayleigh cooling. In addition, the low-level flow is smoothed when the variables are interpolated in the new coordinates. This procedure leads to some weakening of the fast-moving vortices in spite of diabatic heating.

3. Description of numerical experiments

The numerical experiments described below are designed to examine how the development of dynamic instabilities, and the subsequent changes in the cyclone motion, depend on the structure of an initial vortex and the form of the environmental forcing. In particular, we try to answer the following questions:

- Do the unstable modes observed in a linear shallow-water model also appear in a three-dimensional primitive equation model?
- Can the influence of outflow-layer instabilities be identified in the vortex path?
- How is the development of instabilities and resulting vortex motion dependent on environmental forcing?

In the first set of experiments we look for spontaneous development of dynamic instabilities in model vortices and assume the initial flow in the form of superposition of a symmetric vortex and prescribed, environmental asymmetric flow. Since our interest lies mainly in $s = 1$ asymmetries, the environmental flow is very simple and consists of vertically and horizontally uniform easterly flow with $U = -1$ m s^{-1}.

In the second set of experiments, the interaction between a symmetric vortex and time-dependent environmental forcing is examined. In these experiments we neglect the initial asymmetric component of environmental flow but include the upper-layer asymmetric forcing. We study the development of asymmetries in response to forcing and look for resonance between oscillating forcing and barotropically unstable modes. The estimation of the frequency of unstable modes is based on the results from the shallow-water model (Flatau and Stevens 1989). In our shallow-water model, the critical radius (i.e., the radius where the frequency of the unstable mode equals the angular velocity of the flow) was located near the inflection point (i.e., the radius where the potential vorticity gradient changes sign). Therefore, for the purpose of this calculation, we assume that the frequency of the unstable mode is close to the angular velocity at the inflection point ($r = r_B$). The additional momentum forcing term included in governing equations has the form

$$F_u = u_{\text{ref}}/T_{\text{ref}} \cos(\omega_F t) \exp(-(r - r_h)^2/r_0^2) \quad (5)$$

$$F_v = -iF_u, \quad (6)$$

where F_u and F_v denote the radial and azimuthal forcing, respectively, $u_{\text{ref}} = 1$ m s^{-1} and $T_{\text{ref}} = 24$ h. The forcing has the form of an $s = 1$ asymmetry and can either speed or slow the flow along the x axis. The forcing term has a Gaussian distribution in the radial direction with the half-width r_0 and the maximum at $r = r_h$. Since our emphasis is on the dynamical processes in the upper layer, the forcing term is included only in the upper troposphere ($\sigma = 0.3$ corresponding to 300-mb level). Therefore, all the asymmetric components of the low-level flow result from interaction between upper and lower levels. In the experiments we vary the frequency and horizontal distribution of the forcing.

Numerical experiments are carried out for two types of vortices. Vortex A has large tangential velocities ($V_{\max} = 30$ m s^{-1}) and satisfies the criteria for barotropic (potential vorticity gradient reversal on an isentropic surface) and inertial (negative potential vorticity) instabilities in the upper layers (Fig. 1a). There is a region with negative potential vorticity located near $r_{B1} = 200$-km radius in the middle and upper layers. The vorticity gradient changes sign in this area. The reversal of potential vorticity gradient can be also observed in the upper layers (300–200 mb) at about $r_{B2} = 550$-km radius. At this radius the tangential velocity plot indicates that angular velocity is equal to about -1.2×10^{-5} s^{-1} (corresponding to the period of 140 h). For another potential vorticity minimum at r_{B1}, which extends from about 500 to 200 mb, the angular velocity varies from 1.0×10^{-5} s^{-1} at 300 mb to 4×10^{-5} s^{-1} at 500 mb. Vortex B (Fig. 1b) has small

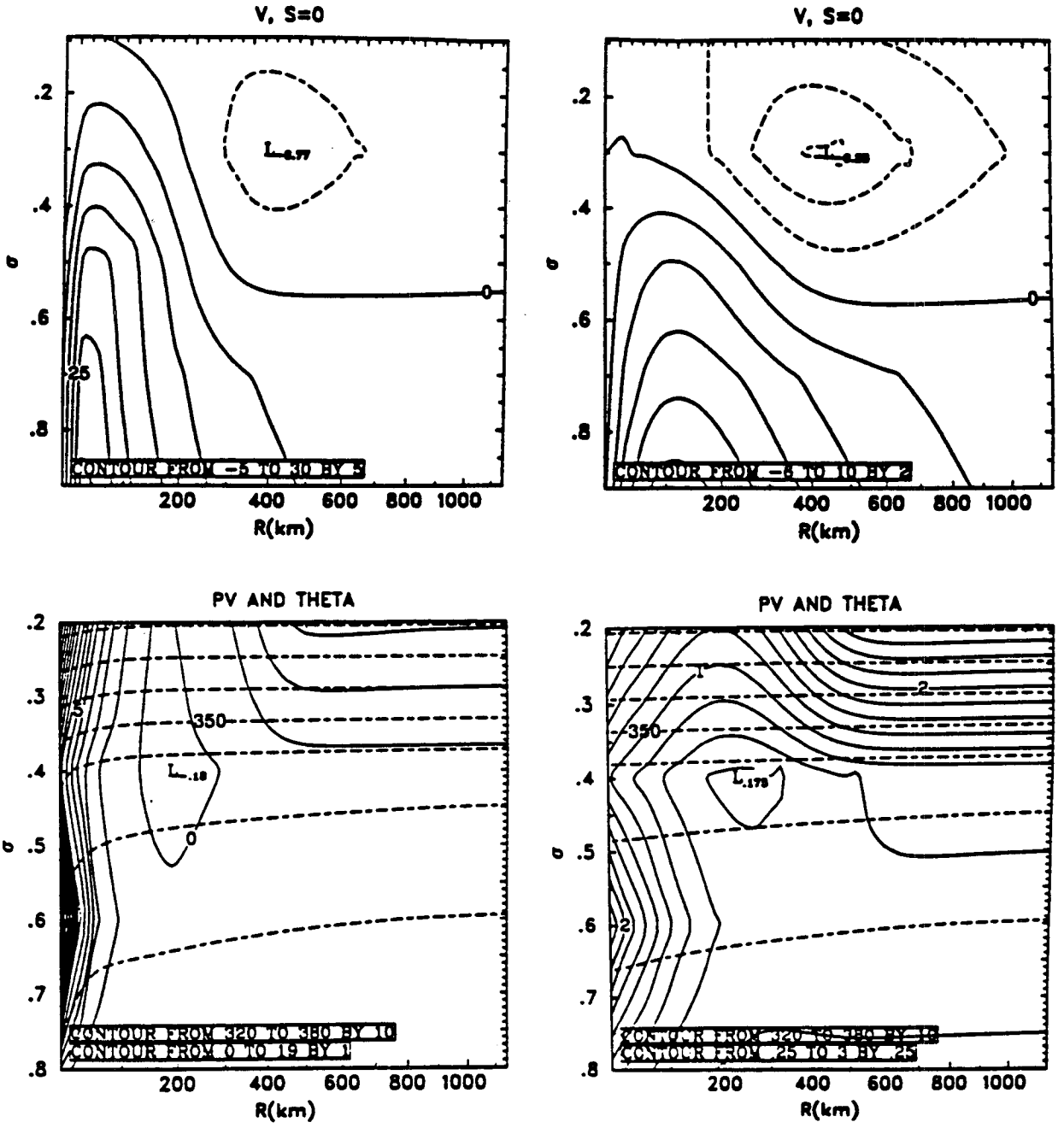

FIG. 1. Initial symmetric vortices—tangential wind, potential vorticity, and potential temperature (dashed lines). (a) The strong vortex (vortex A); (b) the weak vortex (vortex B).

(V_{max} = 10 m s^{-1}) tangential velocities and is inertially stable. In this case there is a region of potential vorticity reversal about 250 km from the center. The angular velocities at this radius are rather small (7.5 × 10^{-6} s^{-1}), corresponding to periods of about 230 h (9.6 days).

All experiments are listed in Table 1. To identify the instability in our baroclinic vortex model we look for features in vortex track and vortex velocity that have time dependency corresponding to the estimated frequency of unstable modes.

a. Motion in a steady environmental flow

First the motion of baroclinic vortices in a steady environmental flow is considered. In experiments I and II we assume that there is no time-dependent environmental forcing and that therefore resonance is not pos-

TABLE 1. List of experiments.

Experiment	Vortex	Initial wind	Forcing
I	B	$u = 1$ m s^{-1}	0
II	A	$u = 1$ m s^{-1}	0
III	B	0	$r_h = 500$ km. $T_F = 140$ h
IV	A	0	$r_h = 500$ km. $T_F = 140$ h
V	A	0	$r_h = 500$ km. $T_F = 43$ h
VI	A	0	$r_h = 500$ km. $T_F = 14$ h
VII	A	0	$r_h = 200$ km. $T_F = 43$ h
VIII	A	0	$r_h = 200$ km. $T_F = 43$ h, $H_F = 500$ mb
IX	A	0	$r_h = 500$ km. $T_F = 140$ h, stronger diabatic heating
X	A	0	$r_h = 500$ km. $T_F = 140$ h, nudging

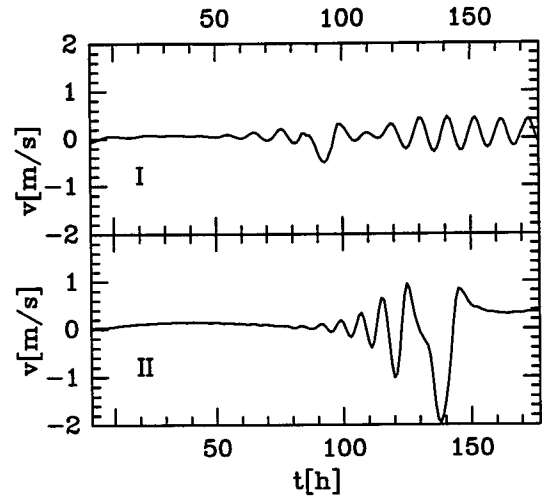

FIG. 3. Meridional vortex velocity for weak (experiment I) and strong (experiment II) vortex in uniform environmental wind field $u = -1$ m s^{-1}.

sible. The environmental flow, however, provides the initial asymmetric $s = 1$ components, which can grow in the presence of barotropic instability. Figures 2 and 3 show the vortex tracks and meridional vortex velocities for experiments I (weak vortex) and II (strong vortex). In a steady easterly flow (-1 m s^{-1}) both vortices experience cyclonic looping motion with amplitudes of about 100 km. The velocity diagram (Fig. 3) indicates that trochoidal, cyclonic oscillations develop early in the weak vortex, while the strong vortex moves with the environmental flow for about the first 80 h. The maximum amplitude of these oscillations is slightly larger for the strong vortex, but it decays rapidly after 150 h. To identify the source of these oscillations we calculated the power spectrum of kinetic energy of the vortex motion (Fig. 4). It can be seen that both vortices experience oscillations with relatively short periods (about 10 h). The periods of these oscillations are much smaller than the periods of possible barotropic oscillations in vortex A or B, and therefore this fast trochoidal motion cannot be related to barotropic instability.

The looping motion with similar periods (a few hours) and amplitudes of a few tens of kilometers can sometimes be detected in real tropical cyclones (Jordan 1966; Muramatsu 1986). Muramatsu (1986) observes that oscillations occur in a double-eye stage of a cy-

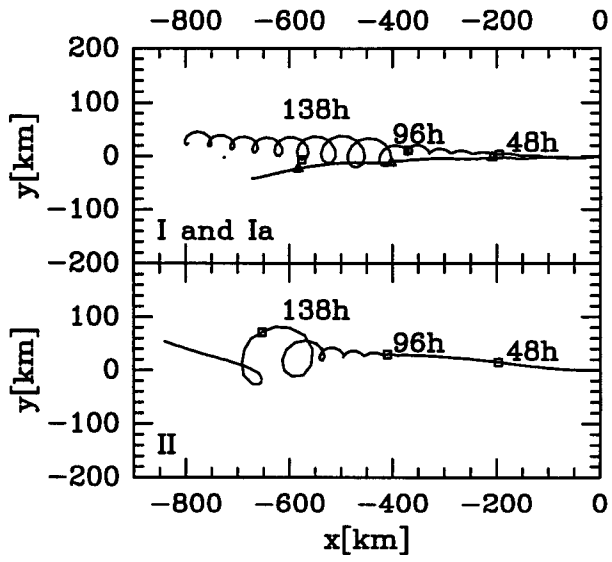

FIG. 2. Vortex track for weak (experiments I and Ia) and strong (experiment II) vortex in uniform environmental wind field $u = -1$ m s^{-1}.

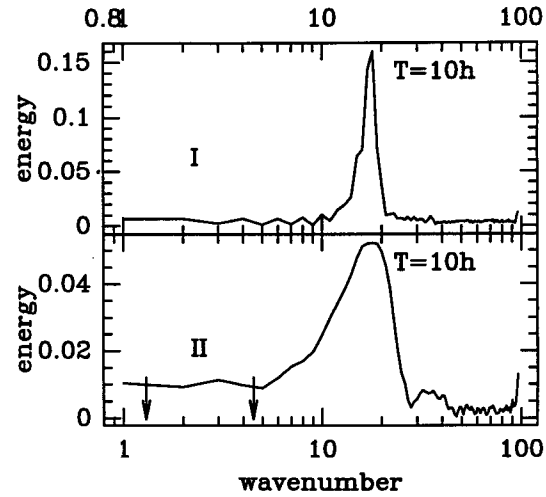

FIG. 4. Power spectrum for the weak (experiment I) and strong (experiment II) vortex. The energy is normalized to the total kinetic energy of the vortex motion. The wavenumbers are plotted on logarithmic scale. The period T of the mode with wavenumber n is equal to $T_n = L/(n)$, where $L = 8$ days. The arrows denote the barotropically unstable modes in vortex A.

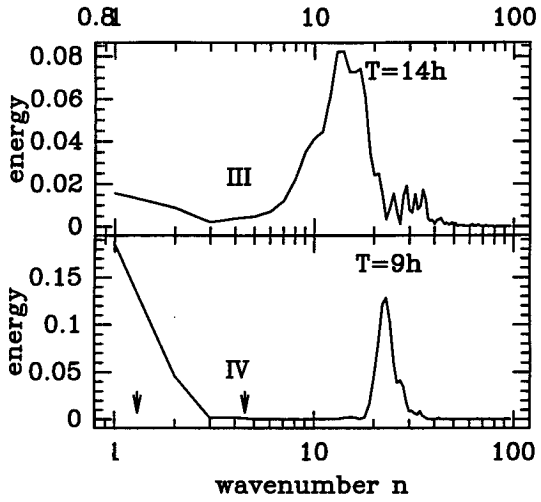

FIG. 5. Power spectrum for experiments III (weak vortex) and IV (strong vortex). The energy is normalized to the total kinetic energy of the vortex motion. The wavenumbers are plotted on logarithmic scale. The period of the mode with the wavenumber n is $T = L/n$, where $L = 8$ days. The arrow denotes the barotropically unstable modes in vortex A.

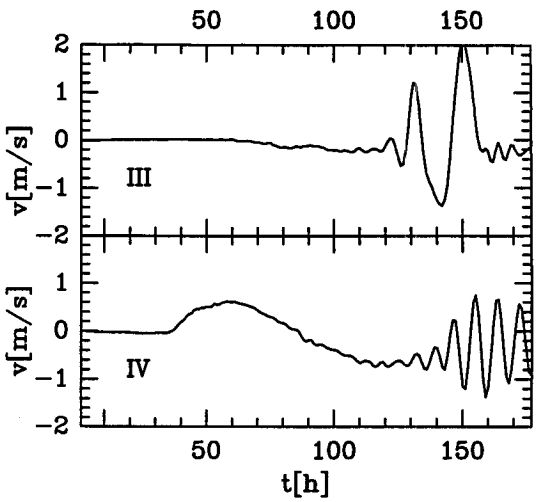

FIG. 6. Meridional vortex velocity for experiments III (vortex B—weak) and IV (vortex A—strong).

clone, which is when the center of the inner eye does not coincide with the center of a larger-scale circulation. He concludes that trochoidal oscillation is possible whenever the inner region of a cyclone becomes asymmetric.

This type of oscillation is not connected with dynamical instabilities but results from the imbalance between the pressure gradient and centrifugal force. Therefore, it should be easier to excite in weaker vortices, since in an intensive vortex the high inertial stability inhibits the development of asymmetric flow. The mechanism of such oscillations was first described by Yeh (1950), who has shown that a vortex in solid-body rotation, moving in uniform zonal flow with velocity U, moves along a trochoidal path. The amplitude and frequency of trajectory oscillations depend on intensity and size of a vortex. According to Yeh, the small, intense vortices have larger frequencies but smaller amplitudes of oscillations than large, weak vortices. Yeh's results are rather difficult to compare with the observations because his calculations are highly idealized and involve assumptions about the vortex characteristics. The observed trajectories of the storms tend to have amplitudes similar to these predicted by Yeh, but much smaller frequencies (Horn 1951).

The processes leading to the development of double-eye structure can be difficult to identify (Muramatsu 1986). In some numerical models (Jones 1987) the trochoidal motions appear before the cyclone landfall. This suggests that the influence of land causes the asymmetries of a low-level circulation and oscillation in the cyclone track. In our model, the source of asymmetry between momentum and the pressure field is connected to convective heating. Even though the heating is assumed to be symmetric relative to the vortex center, the fact that it is adjusted to the pressure field in discreet time intervals (every hour) can disturb the gradient balance in the vortex and introduce small asymmetries. To test this hypothesis, an additional experiment (Ia) is run in which we neglect the diabatic heating. As can be seen in Fig. 2, the vortex in this case moves along the straight line, and trochoidal motion disappears.

The very sharp and narrow peak in the power spectrum of the weak vortex in experiment I indicates that for the weak vortex the stable oscillation is the sole

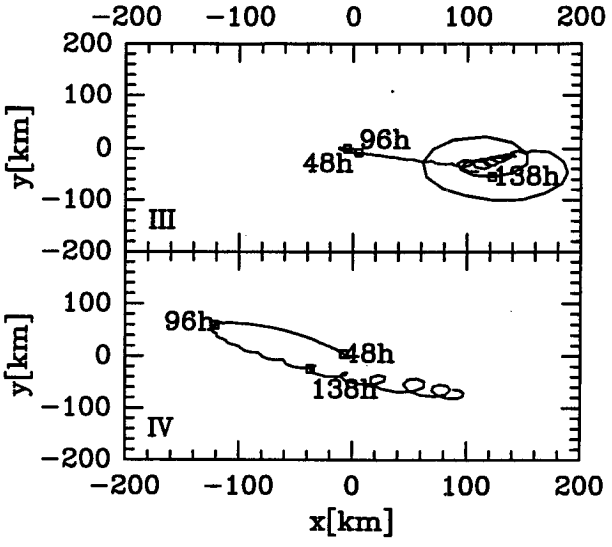

FIG. 7. Vortex track in experiments III and IV.

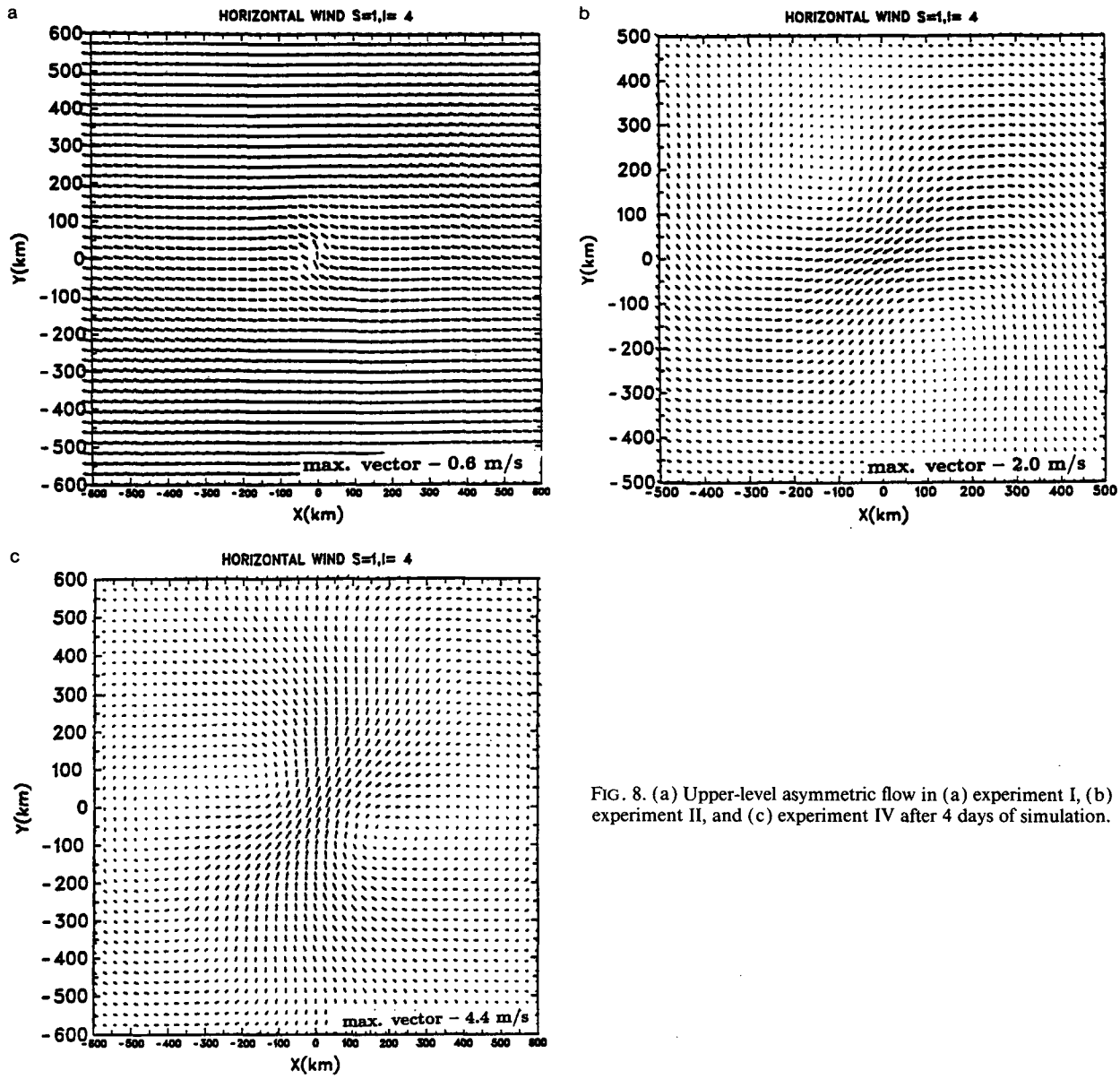

FIG. 8. (a) Upper-level asymmetric flow in (a) experiment I, (b) experiment II, and (c) experiment IV after 4 days of simulation.

internal mechanism responsible for looping. There is no energy in the low-frequency modes corresponding to barotropic instability. For the strong vortex the power spectrum is much broader. Even though cyclonic looping with large frequencies dominates, there is a small peak near the frequency of $-1.2 \times 10^{-5}\ s^{-1}$ corresponding to barotropic instability (it is difficult to detect on the power spectrum diagram but is clearly present in the data).

Our goal is to determine if there is a forcing that excites oscillations with this frequency. Because the phase speed for the barotropically unstable modes can be negative (i.e., perturbations propagate anticyclonically), such oscillations could be responsible for anticyclonic as well as cyclonic turning of the vortex. As shown by Holland (1991) and Xu and Gray (1982), both cyclonic and anticyclonic looping motion is observed in tropical storms. Additionally, Holland (1988) suggests that the development of barotropically unstable modes can affect recurvature of a cyclone.

b. *Motion with environmental forcing*

In the next set of experiments we try to excite the barotropically unstable modes using a time-dependent momentum forcing. The forcing has the form given by Eq. (6). At first, we choose the frequency of the forcing that corresponds to one of the barotropic instability frequencies in the strong vortex ($\omega_F = -1.2$

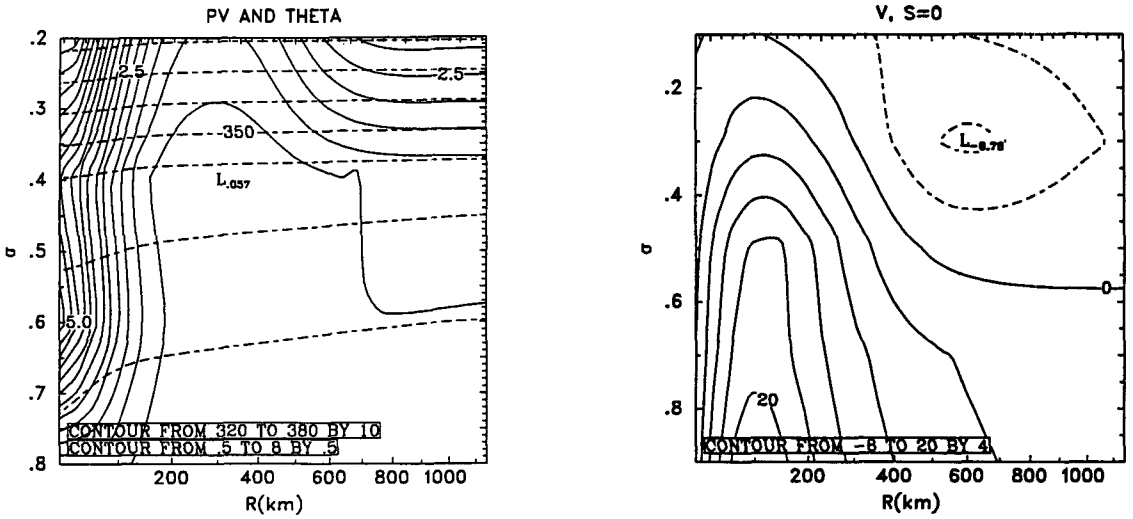

FIG. 9. The mean tangential flow and potential vorticity in the strong vortex after 4 days of integration (experiment IV).

$\times 10^{-5}$, $T_F = 140$ h); the same forcing is used for both vortices.

As can be seen from Fig. 5, the response of both vortices to the identical forcing is quite different. In the case of the strong vortex (vortex A, experiment IV), most energy (about 20%) is concentrated in the modes with the lowest frequency, corresponding to the frequency of the forcing. For the weaker vortex (vortex B, experiment III), the modes with periods of about 14 h contain the most energy. Only 2% of the energy is contained in the low-frequency modes. Since the barotropically unstable modes in vortex B should have the period on the order of a few days, this suggests that barotropic instability does not develop in the weak vortex.

The difference of the response can be seen also in vortex velocity. In both cases, the zonal velocity corresponds to forcing, but the response is stronger and appears earlier in the strong vortex. The meridional velocity of the weak vortex stays close to zero until about 140 hours of integration (when cyclonic loops appear), while meridional velocity for the strong vortex changes in response to the forcing (Fig. 6). The tracks of the two vortices are also quite different (Fig. 7). The stronger vortex first makes the slow loop, while the weak vortex stays motionless. After about 5 days both vortices experience fast, cyclonic looping motion, although the loops are larger for the weaker vortex.

To further investigate the nature of the dynamic process that causes the looping in experiment IV, we compare the upper-level asymmetric flow in experiments I, II, and IV (Fig. 8). The upper-layer asymmetric flow confirms our conclusion that barotropic instability was the reason for slow looping motion in experiment IV. For the weak vortex in experiment I, the flow in the upper layer is very similar to the initial environmental flow. In the strong vortex in a steady environment (experiment II), the amplification of the asymmetric flow can be seen near the vortex center—a structure similar to that observed in barotropically unstable modes in the shallow-water model. The upper-layer flow is stronger than the initial flow and concentrated near the vortex center. The asymmetric wind in experiment IV has a structure similar to that observed in experiment II, but the amplitude of an asymmetric component of an upper-level flow is much larger.

The mean, upper-level flow does not change significantly during the integration (Fig. 9). The magnitude of the anticyclonic flow in the outflow layer after 96 h of calculation is similar to that of the initial flow, with the maximum of 9 m s^{-1}. The low-level flow is weakened to 22 m s^{-1}. Both inflection points still appear in the potential velocity field at radii 300 and 800 km. This change of the tangential flow causes a slight decrease of frequency for the mode with the negative phase speed (period increases from 140 to 170 h) and more marked decrease of frequency for the mode with positive phase speed (the period doubles).

It is worth noting that the slow loop in the track of vortex A is cyclonic, even though the low frequency of this motion suggests that it is connected to the barotropically unstable mode with the negative phase speed. As seen in Fig. 10, however, the asymmetric flow in the upper layer turns anticyclonically, as would be expected for a barotropic instability with this frequency.

In the next two experiments, the response of a strong vortex (vortex A) to different frequency forcing is investigated. The goal of these experiments is to determine if the vortex response is stronger when the forcing frequency matches that of the barotropically unstable mode. In experiment V (Fig. 11) we use the frequency

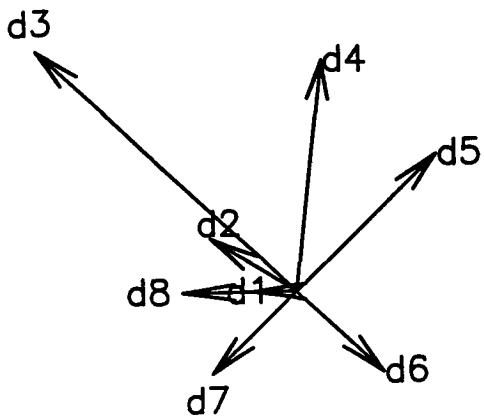

FIG. 10. Upper-level asymmetric flow, near the vortex center in experiment IV. The length of arrows is proportional to the asymmetric wind velocity at the vortex center. The symbol d1 denotes the first 24 h of calculations, d2 the second day, etc.

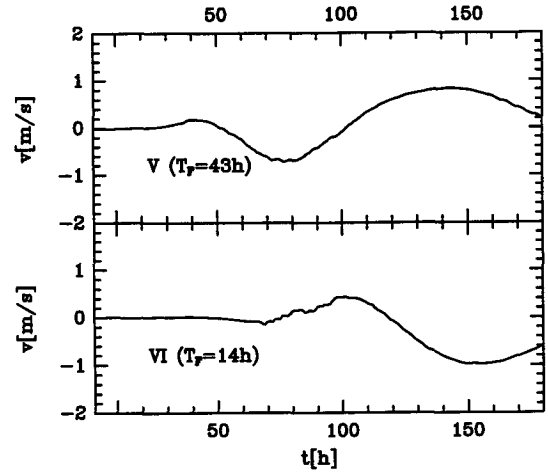

FIG. 12. Meridional vortex velocity in experiments V and VI.

$\omega_F = 5. \times 10^{-5}$ ($T_F = 43$ h) corresponding to the frequency of the cyclonically propagating unstable mode in vortex A. In experiment VI we use the forcing frequency $\omega_F = 1. \times 10^{-4}$ ($T_F = 14$ h), which is not connected to barotropic instability frequency in either of the vortices. As can be seen from Fig. 12, when the forcing frequency is larger than the frequency of the unstable modes, the vortex initially does not move. After 70 h, however, the vortex starts a slow looping motion with the period of about 100 h (Fig. 13). The development of this motion can be explained by the fact that the stationary vortex intensifies faster and that after about 3 days of integration the cyclonic, angular velocity near the inflection point reaches the magnitude of the forcing frequency. It is worth noting, however, that the period of the looping motion that develops after 70 h is much larger than the period of the forcing and corresponds to the frequency of the other anticyclonically propagating mode. In experiment V, when the slower forcing is applied, the vortex responds much faster. Nevertheless, in both experiments the response of the vortices is concentrated in the frequencies smaller than the forcing frequency (Fig. 11). In experiment V ($T_F = 43$ h) there is a small peak corresponding to the forcing frequency, but most of the response is contained in the motion with periods above 100 h.

Since the frequency of the vortex response in experiments V and VI is similar to the angular velocity at the radius of maximum forcing ($r = r_{B2} = 500$ km), in the next two experiments we change the horizontal distribution on the forcing function. The maximum forcing is now placed at $r = r_{B1} = 200$ km, and the

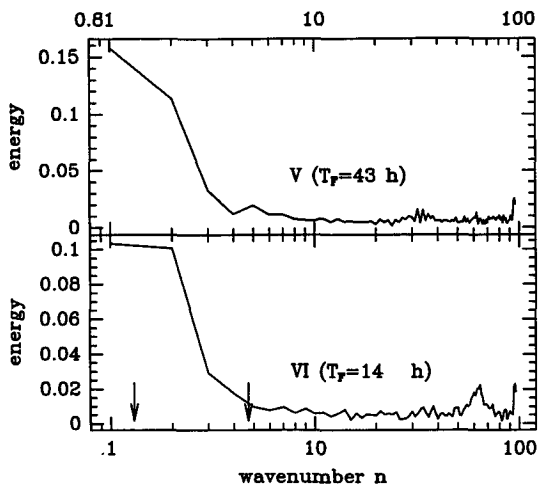

FIG. 11. Power spectrum for experiment V ($T_F = 34$ h) and VI ($T_F = 14$ h).

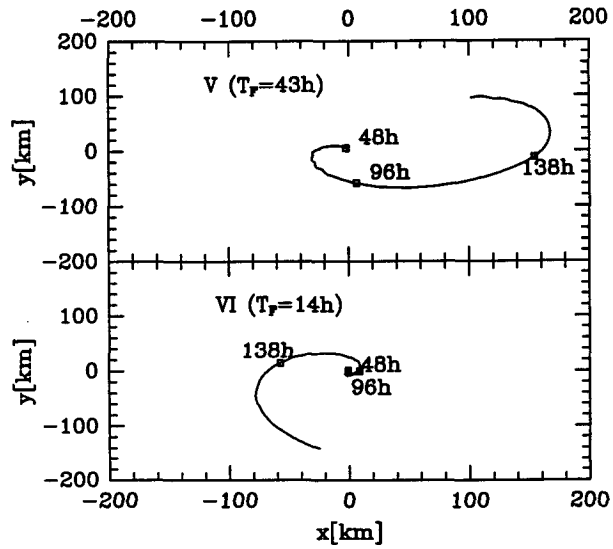

FIG. 13. Vortex track in experiments V and VI.

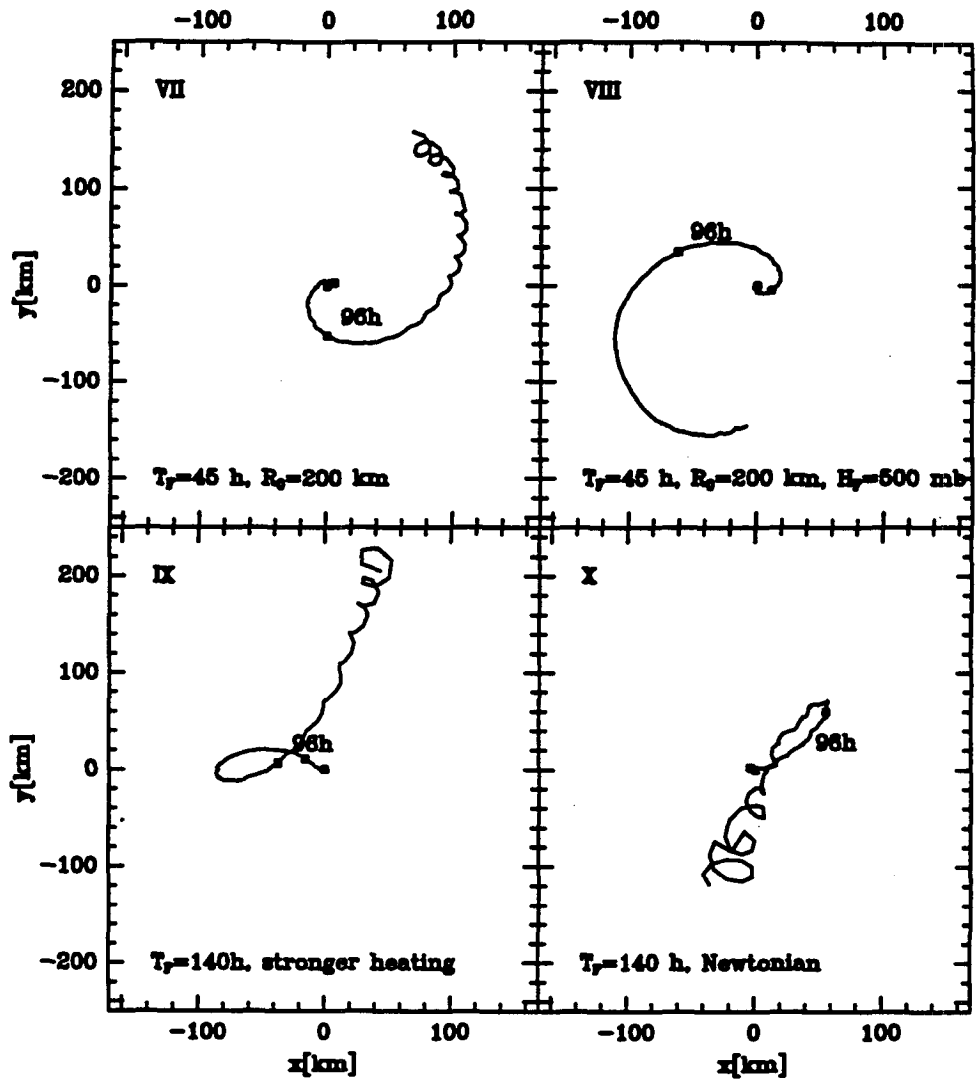

FIG. 14. Vortex track in experiments VII–X.

vortex A (strong vortex) is used as an initial condition. In vortex A the angular velocity at 200 km, especially at lower levels (500 mb), is larger than angular velocity at r = 500 km. Here we want to determine if the frequency of the response increases to correspond to the angular velocity at the radius of maximum forcing. The forcing period is equal to 43 h; that is, the frequency of the forcing matches the angular velocity at 500 mb and r = 200 km. In experiment VII the forcing is limited to the upper (σ = 0.3) troposphere, while in experiment VIII the forcing is placed at the 500-km level. In spite of this type of forcing, the period of a slow looping motion in experiments VII and VIII is similar to that observed in the previous experiments. Therefore, we can conclude that the frequency of the response is determined by the characteristics of the vortex rather than distribution of the environmental forcing (Fig. 14).

The next experiment (experiment IX) is another version of experiment IV: The forcing is the same as in experiment IV (T_F = 140 h, r_h = 500 km), and vortex A is used as an initial state, but the basic vortex is modified by increasing the diabatic heating rate by 1.5. As could be expected, since the vortex remains stronger ($V_{max} > 30$ m s^{-1}), the frequency of the slow, as well as the fast, looping motion is slightly increased compared to those in experiment IV.

In the last experiment (X), experiment IV is essentially repeated, but instead of the forcing being independent of the flow characteristic, we assume the forcing is in the form of Newtonian "nudging"; that is,

$$F_u = (-u - u_{\text{ref}})/T_{\text{ref}} \cos(\omega_F t) \exp(-(r - r_h)^2/r_0^2). \quad (7)$$

The vortex track is similar to that in experiment IV,

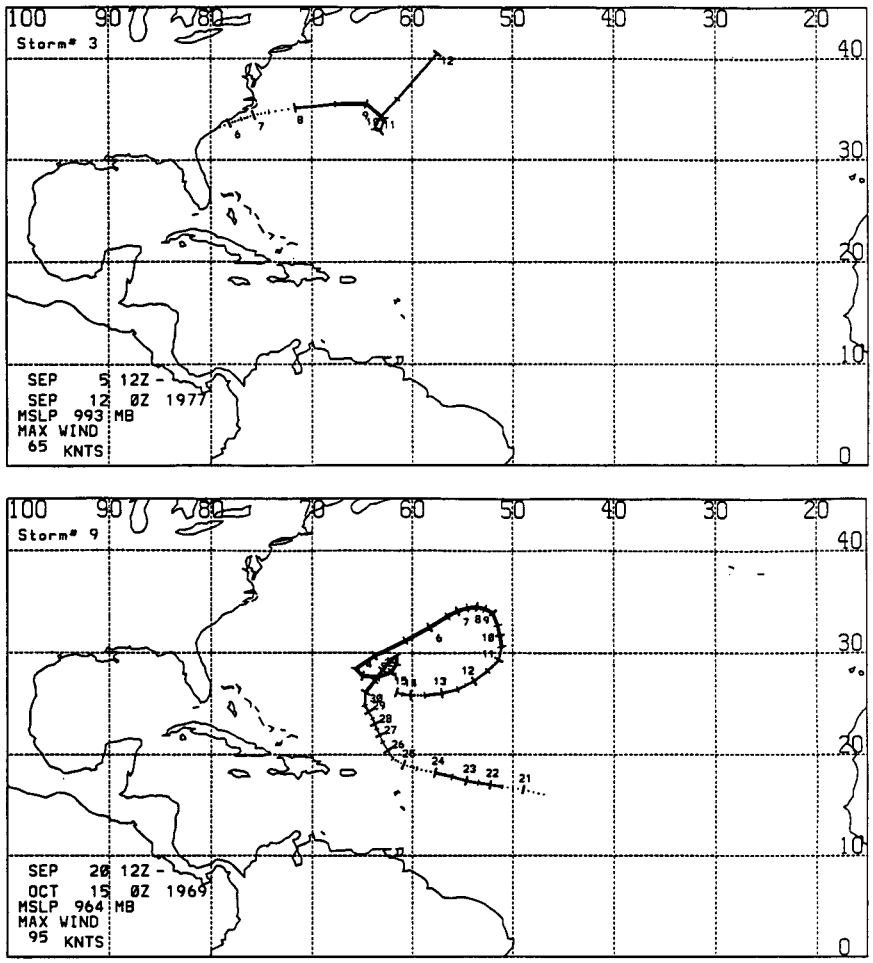

FIG. 15. The examples of anticyclonically looping tropical cyclones for (a) Hurricane Clara and (b) Hurricane Inga.

but the slow loop is anticyclonic instead of cyclonic like in experiment IV.

4. Summary

We have examined the influence of barotropic instability developing in an outflow layer of a three-dimensional vortex on the motion of a vortex. We identified barotropic instability by comparing the frequency of the free, unstable barotropic modes with the frequency of a trochoidal motion of the vortices. In our results two types of trochoidal motion are found. The first type, always cyclonic, with periods of about 10 h, was observed in both strong and weak vortices. We concluded that this type of motion was associated with a stable oscillation resulting from the imbalance between pressure gradient and centrifugal force. This type of oscillation can be found in observed (Jordan and Stovell 1955; Horn 1951; Muramatsu 1986) as well as modeled (Jones 1987) storms. The oscillations are usually observed during landfall and are often accompanied by the double-eye structure. A similar type of motion was also observed in Willoughby's (1988) linear model of tropical cyclone motion, when the mass sink–source simulating the asymmetry of convection was included.

We also observed the slow looping motion, with the large periods corresponding to the period of barotropically unstable mode. This type of trochoidal path was found only in the intense vortex. Even though there were two inflection points in potential vorticity in this vortex, the response of the vortex was always concentrated near the slower mode, which had a critical radius located near the maximum anticyclonic velocity of an upper-layer flow. The special role of this frequency was also noted by Willoughby (1988). In his linear, shallow-water model, the forcing that corresponded to this frequency caused the resonant response and large deflection of the vortex track from the environmental flow.

Loops with periods of a few days, similar to those that developed in our simulations, can sometimes be observed in real cyclones (Xu and Gray 1982). Figure

15 shows two examples of such tracks. The looping storms in Fig. 15 were intense, such that barotropic instability could have developed in their outflow layers, contributing to the looping motion. As noted by Xu and Gray (1988), the typical synoptic situation for the looping motion of tropical storms involves temporal changes in the environmental flow (e.g., deepening midlatitude trough or rapidly moving short-wave trough). Therefore, the environment can provide the forcing necessary to trigger the unstable mode. Since the changing environmental flow also advects the vortex, it is difficult to say without careful analysis of the storm structure which mechanism dominates. Nevertheless, the difference in the response to the same environmental forcing for the strong and weak vortices shows that a tropical cyclone is not merely advected by the environmental flow but that the internal dynamics contributes to its motion.

Acknowledgments. The authors are grateful to Dr. Wayne Schubert and Dr. William Gray, to Paul Ciesielski, and to the anonymous reviewers for their helpful comments and discussion. This work was sponsored by NSF under Grants ATM8352205 and ATM8609731 and by the Office of Naval Research under Grant N000014-K-0214. The computing support was provided by the National Center for Atmospheric Research.

APPENDIX

Calculation of Potential Vorticity in σ Coordinates

Potential vorticity is given by

$$P = (\boldsymbol{\zeta}_a + f\mathbf{k}) \cdot \nabla\theta \frac{1}{\rho}, \tag{8}$$

where $\boldsymbol{\zeta}_a$ denotes absolute vorticity. Vorticity in cylindrical coordinates (r, λ, z) can be expressed as

$$\boldsymbol{\zeta}_a = \mathbf{k}\left[\frac{1}{r}\left(\frac{\partial(rv)}{\partial r} - \frac{\partial u}{\partial \lambda}\right) + f\right] + \boldsymbol{\lambda}\left(\frac{\partial u}{\partial z}\right) + \mathbf{r}\left(-\frac{\partial v}{\partial z}\right), \tag{9}$$

where derivatives of vertical velocity were omitted, because of the hydrostatic assumption. Using (9), we express potential vorticity in cylindrical coordinates as

$$P = \frac{1}{\rho}\left[f + \left(\frac{\partial rv}{\partial z} - \frac{\partial u}{\partial \lambda}\right)\right]\frac{\partial\theta}{\partial z} + \frac{1}{r\rho}\frac{\partial u}{\partial z}\frac{\partial\theta}{\partial\lambda} - \frac{1}{\rho}\frac{\partial v}{\partial z}\frac{\partial\theta}{\partial r}. \tag{10}$$

Transformation to σ coordinates is given by the following expressions:

$$\left(\frac{\partial x}{\partial r}\right)_z = \left(\frac{\partial x}{\partial r}\right)_\sigma + \frac{\sigma}{RT}\left(\frac{\partial\phi}{\partial r}\right)_\sigma \frac{\partial x}{\partial\sigma}$$

$$\left(\frac{\partial x}{\partial \lambda}\right)_z = \left(\frac{\partial x}{\partial r}\right)_\sigma + \frac{\sigma}{RT}\left(\frac{\partial\phi}{\partial \lambda}\right)_\sigma \frac{\partial x}{\partial\sigma} \tag{11}$$

$$\left(\frac{\partial x}{\partial z}\right) = -\frac{\partial x}{\partial\sigma}\frac{\rho g}{p_s}. \tag{12}$$

Combining (12) and (10) we obtain the expression for potential vorticity in σ coordinates (r, λ, σ):

$$P = \left\{\frac{1}{r}\left[\frac{\partial rv}{\partial r} - \frac{\partial u}{\partial\lambda} + \frac{\sigma}{RT}\left(\frac{\partial\phi}{\partial r}\frac{\partial rv}{\partial\sigma} - \frac{\partial\phi}{\partial\lambda}\frac{\partial u}{\partial\sigma}\right)\right] + f\right\}$$
$$\times\left(-\frac{\partial\theta}{\partial\sigma}\frac{g}{p_s}\right) - \frac{g}{rp_s}\frac{\partial u}{\partial\sigma}\left(\frac{\partial\theta}{\partial\lambda} + \frac{\sigma}{RT}\frac{\partial\phi}{\partial\lambda}\frac{\partial\theta}{\partial\sigma}\right) \tag{13}$$

$$+\frac{g}{p_s}\left(\frac{\partial\theta}{\partial r} + \frac{\sigma}{RT}\frac{\partial\phi}{\partial r}\frac{\partial\theta}{\partial\sigma}\right). \tag{14}$$

The potential vorticity fields in this paper are presented using the normalized potential vorticity $P_n = P/P_{nn}$, where normalization factor P_{nn} is given by

$$P_{nn} = -f_0\frac{\theta(\sigma_T) - \theta(\sigma_B)}{(\sigma_T - \sigma_B)}\frac{g}{p_0}. \tag{15}$$

REFERENCES

Black, P. G., and R. A. Anthes, 1971: On the asymmetric structure of the tropical cyclone outflow layer. *J. Atmos. Sci.*, **28,** 1348–1366.

DeMaria, M., 1987: Tropical cyclone motion in a nondivergent barotropic model. *Mon. Wea. Rev.*, **115,** 2346–2357.

Emanuel, K. A., 1989: The finite-amplitude nature of tropical cyclogenesis. *J. Atmos. Sci.*, **46,** 3431–3456.

Flatau, M., and D. E. Stevens, 1989: Barotropic and inertial instabilities in a hurricane outflow layer. *Geophys. Astrophys. Fluid. Dyn.*, **47,** 1–18.

Hack, J. J., and W. H. Schubert, 1980: The role of convective-scale processes in tropical cyclone development. Atmos. Sci. Paper 330, Colorado State University, 206 pp.

——, and ——, 1986: Nonlinear response of atmospheric vortices to heating by organized cumulus convection. *J. Atmos. Sci.*, **43,** 1559–1573.

Holland, G. J., 1988: General recurvature forecast problems. *ONR Tropical Cyclone Motion Research Initiative: First Year Review.* Prepared for Chief of Naval Research, 18–22.

——, 1991: On the meandering nature of tropical cyclone tracks. Proc. *19th Conf. on Hurricanes and Tropical Meteorology,* Amer. Meteor. Soc., Miami., 53–55.

Horn, J. D., 1951: On irregular movements of tropical cyclone in the Pacific. *Bull. Amer. Meteor. Soc.*, **32,** 344–345.

Jones, R. W., 1977: A nested grid for a three-dimensional model of a tropical cyclone. *J. Atmos. Sci.*, **34,** 1528–1553.

Jones, W. R., 1987: A simulation of hurricane landfall with a numerical model featuring latent heating by resolvable scales. *Mon. Wea. Rev.*, **115,** 2279–2297.

Jordan, C. L., 1966: Surface pressure variations at coastal stations during the period of irregular motion of hurricane Carla of 1961. *Mon. Wea. Rev.*, **94,** 454–458.

——, and D. J. Stovell, 1955: Some small-scale features of the track of hurricane Ione. *Mon. Wea. Rev.*, **83,** 210–215.

Kitade, T., 1980: Numerical experiments of tropical cyclones on a plane with variable Coriolis parameter. *J. Meteor. Soc. Japan,* **58,** 471–488.

Muramatsu, T., 1986: Trochoidal motion of the eye of typhoon 8019. *J. Meteor. Soc. Japan,* **64,** 259–272.

Peng, M. S., and R. T. Williams, 1990: Dynamics of vortex asymmetries and their influence on a vortex motion on a β plane. *J. Atmos. Sci.*, **47,** 1987–2003.

Schubert, W. H., and J. J. Hack, 1983: Transformed balanced vortex model. *J. Atmos. Sci.*, **30,** 1571–1583.

——, and B. T. Alworth, 1987: Evolution of potential vorticity in tropical cyclones. *Quart. J. Roy. Meteor. Soc.*, **113,** 147–162.

Willoughby, H. E., 1988: Linear motion of a shallow-water, barotropic vortex. *J. Atmos. Sci.*, **45,** 1906–1928.

Xu, J., and W. M. Gray, 1982: Environmental circulations associated with tropical cyclones experiencing fast, slow and looping motion. Atmos. Sci. Paper 346, Colorado State University, 110 pp.

Yanai, M., S. Esbensen, and J. Chu, 1973: Determination of bulk properties of tropical cloud clusters from large-scale heat and moisture budgets. *J. Atmos. Sci.*, **30,** 611–627.

Yeh, T. C., 1950: The motion of tropical storms under the influence of a superimposed southerly current. *J. Meteor.*, **7,** 108–113.